Proceedings of the 38th Chinese Control Conference
July 27-30, 2019, Guangzhou, China

Control of PEMFC Air Supply Subsystem Using Triple-Step Method

Meng Li[1,2], Yu Zhang[1,2], Yunfeng Hu[1,2] Jinwu Gao[1,2]

1. State Key Laboratory of Automotive simulation and control
E-mail: mengli17@mails.jlu.edu.cn

2. Department of Control Science and Engineering, Nanling Campus Jilin University, Changchun, 130022 China
E-mail: gaojw@jlu.edu.cn

Abstract: In this paper, the control targets are the flow rate into the cathode and the pressure of the cathode. Firstly, the typical structure of the proton-exchange membrane fuel cell (PEMFC) air supply subsystem is briefly introduced and a simplified multi-input and multi-output (MIMO) air supply subsystem of a PEMFC is proposed. Then optimize the tracking targets under different load currents and establish a map between load current and tracking targets. Finally a nonlinear controller called the triple-step method is designed and the stability of the system is proved by Lyapunov stability theory. The simulation results show good performance that the system can quickly track the targets with no steady-state error when tracking targets and load current step-change.

Key Words: Fuel Cell, Air Supply Subsystem, Triple-step Method, Optimization

1 Introduction

Fuel cells are a form of clean and high-efficiency power source without carbon emission. Among all sorts of Fuel cells, the PEMFC attracts much attention from the fields of portable and automotive application. Especially for the automobile industry, PEMFC is regarded as the most potential candidate to replace conventional internal combustion engines for its low working temperature, quick start-up, zero emission.

There are four main subsystems in a typical PEMFC system (see Figure 1)[1]: air supply subsystem, hydrogen supply subsystem, temperature and humidity management subsystem and energy management subsystem. Among these subsystems, the air supply subsystem consumes the most electric energy and diminishes the net power of the PEMFC system. The parasitic power required for air supply subsystem can account for 25 percents of the total output power of PEMFC [2]. Air supply system comprises necessary peripheral components such as air compressor, air supply manifold and cathode. Generally, flow rate into the cathode and cathode pressure need to be controlled coordinately to avoid oxygen starvation, stack flooding and provide the maximum net power, maintain appropriate pressure difference between cathode and anode. So air supply subsystem modeling and control are rather important for performance improvement of PEMFC. For a long time in the past, research about air supply subsystem mainly focus on oxygen excess ratio modeling and control. Several different control models have been proposed in previous studies. A nine-order nonlinear model based on electrochemistry, gas dynamics, thermal dynamics proposed by Pukrushpan [3] is widely used and verified. In this model, the dynamic process of the air supply system is described in detail, however the complexity of the model adverse to the control of the system. Through reasonable assumption, nine-order nonlinear model can approximately simplified as four-order model [4]. Based on the work done by Pukrushpan, a third order model is established by Talj [5]. Based on existing models, different effective control strategies have been proposed to control oxygen excess ratio. By linearizing the model, the linear quadratic regulator (LQR) is designed by Pukrushpan [3]. However, due to the uncertainty and the measurement error of high-order model, it is difficult to guarantee the performance of the system because of measurement and nonlinearities. A feedback linearization controller to track variable optimal oxygen excess ratio is proposed by Chen [6]. In this study, mathematical relationship of compressor flow is fitted based on experimental data. and then the control of oxygen ratio is realized and the stability is proved by lyapunov method. A second-order sliding model control is proposed by Kunusch [7]. Although sliding control has a good effect on system uncertainty, the fluctuation is generated near the equilibrium point which is harmful for the system. By optimization, model predictive control (MPC) method is used in the control of oxygen excess ratio [8]. Nevertheless some researchers have found dynamic characteristics (e.g. flow rate into the cathode and cathode pressure) of the PEMFC are more important to meet the power requirements of vehicles in different road conditions and maintain proper pressure difference between cathode and anode.

So far, the researches about coordinated control of flow rate into the cathode and cathode pressure has less been done. A feed-forward approach based on the steady-state plant inverse response, coupled to a multi-variable LQR feedback control is proposed in [9]. However, since the LQR method only works well near linearization point, it is not suitable for vehicles in complex road conditions. [10] designs a Linear Quadratic Gaussian (LQG) control, and Matlab/Simulink simulation is performed to validate the proposed methodology to increase the dynamic performance of a PEMFC system. Based on a simplified control model, using differential flatness control theory, the controller is de-

Corresponding author: Jinwu Gao (gaojw@jlu.edu.cn).

This work was supported by The National Key Research and Development Program of China under Grant 2017YFB0102800, was also supported by the Jilin Provincial Science Foundation of China under Grant 20190302119GX, and Jilin Province Development and Reform Commission Foundation of China under Grant 2019C036-4.

signed to regulate the oxygen excess ratio and the cathode pressure [11]. Based on MIMO system, a controller combining state feedback precise linearization and nonlinear robust control strategy is designed [12], and the experimental results show that the control method can effectively reduce the pressure change caused by the disturbance. In [13], an advanced differential flatness control technology is adopted and tracking observers are used to estimate partial pressure of oxygen.

The main work of this paper is as follows: In the section II, the general structure of the PEMFC air supply subsystem is briefly introduced and a mathematical model of the air supply subsystem has been established. In the section III, a strategy to optimize reference input (flow rate into the cathode and cathode pressure) is proposed based on maximum net power output from PEMFC. In the section IV, a nonlinear control strategy called triple-step method is applied to the system. Simulation results are given in section V. Give conclusions in Section VI.

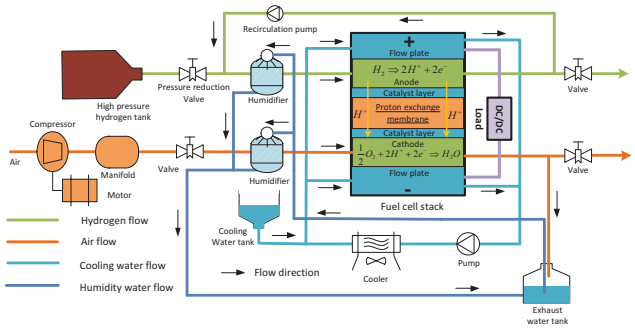

Figure 1: Typical structure of a fuel cell

2 Simulation Model

The simulation model in this paper is based on the modeling work done by literature [3] and [5]. For describing a 45 kw MIMO air supply system, some modifications have been done. A simplified diagram of typical air supply system with three main part is shown in Figure 2: air compressor, air supply manifold and cathode. The air is compressed into the air supply manifold by the air compressor, then flows into the cathode and finally releases into atmosphere through proportional back pressure valve. The flow rate into the cathode and cathode pressure can be regulated by air compressor and proportional back pressure valve.

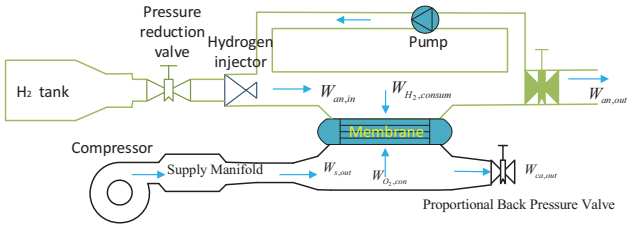

Figure 2: AirChydrogen supply subsystem

2.1 Air Compressor Model

Compressor comprises two parts: blower and electric motor. The impeller of blower is driven by electric motor and compresses the air into air supply manifold. The dynamic characteristics of compressor can be modeled by the combined inertia of electric motor and blower, as well as the torque generated by electric motor. The lumped dynamic model is described as

$$\begin{aligned} \frac{d\omega_{cm}}{dt} &= \frac{1}{J_{cm}}\left(\tau_{cm}-\tau_{cc}\right), \\ \tau_{cm} &= \eta_{cm}\frac{g_a}{R_{cm}}\left(V_{cm}-g_b\omega_{cm}\right), \\ \tau_{cc} &= W_{cm}\frac{C_pT_{atm}}{\omega_{cm}\eta_{cp}}\left[\left(\frac{p_{sm}}{p_{atm}}\right)^{\frac{\gamma-1}{\gamma}}-1\right], \end{aligned} \tag{1}$$

where ω_{cm} and J_{cm} represents the angular velocity of blower impeller and combined inertia of electric motor and blower respectively, τ_{cm} and τ_{cc} are motor torque and required torque by blower respectively, g_a and g_b are variables depended on the compressor specification, V_{cm} is the compressor voltage, R_{cm} is the resistance of blower and electric motor, C_p and p_{sm} represent the specific heat capacity and air supply manifold pressure, η_{cm} and η_{cp} represent motor mechanical efficiency and blower efficiency respectively, p_{atm} and T_{atm} are atmosphere pressure and atmospheric temperature respectively, γ represents ratio of the specific heat capacity of gas, W_{cm} is the air flow rate out of the compressor which is a function of the ratio of air supply manifold pressure, p_{sm}, to atmospheric pressure, p_{atm}, angular velocity, ω_{cm}, of blower impeller in [3] and can be written by

$$W_{cm} = f(\omega_{cm}, p_{sm}). \tag{2}$$

2.2 Air Supply Manifold Model

The air dynamics in air supply manifold is modeled based on the ideal gas law. In the air supply manifold, dynamic characteristics of pressure, p_{sm}, depended on the inlet and outlet flow rates is given as

$$\frac{dp_{sm}}{dt} = W_{sm}\frac{\gamma R_a}{V_{sm}}T_{cm} - W_{s,out}\frac{\gamma R_a}{V_{sm}}T_{cm}, \tag{3}$$

where R_a represents air gas constant, V_{sm} is the volume of air supply manifold, W_{sm} is the flow rate into the air supply manifold approximately equaled to the air flow rate, W_{cm}, the T_{cm} is the temperature of air supply manifold given by

$$T_{cm} = T_{atm} + \frac{T_{atm}}{\eta_{cp}}\left[\left(\frac{p_{sm}}{p_{atm}}\right)^{\frac{\gamma-1}{\gamma}}-1\right], \tag{4}$$

and $W_{s,out}$ is the rate of air flow out of the air supply manifold and then calculated using the nozzle flow equation as

$$W_{s,out} = k_{sc}\left(p_{sm}-p_{ca}\right), \tag{5}$$

where parameter k_{sc} represents nozzle constant. p_{ca} is the cathode pressure.

2.3 Cathode Model

In the cathode, the flowing gas mainly contains oxygen, nitrogen and water vapor. The cathode dynamic equation becomes

$$\frac{dp_{ca}}{dt} = \frac{dp_{O_2}}{dt} + \frac{dp_{N_2}}{dt} + \frac{dp_{vap}}{dt}, \tag{6}$$

where p_{O_2}, p_{N_2}, p_{vap} represent the pressure of oxygen, nitrogen and water vapor respectively. Assuming that water vapor is saturated depended only on temperature of PEMFC, the pressure of water vapor is constant when the PEMFC temperature is a constant, so the pressure dynamic of water vapor is modeled by

$$\frac{dp_{vap}}{dt} = 0, \tag{7}$$

and then according to the ideal gas law and electrochemical theory, the partial pressure dynamics of oxygen and nitrogen can be given as

$$\begin{aligned} \frac{dp_{O_2}}{dt} &= \frac{R_{O_2}T_{st}}{V_{ca}M_{O_2}}\left(W_{O_2,in} - W_{O_2,con} - W_{O_2,out}\right), \\ \frac{dp_{N_2}}{dt} &= \frac{R_{N_2}T_{st}}{V_{ca}M_{N_2}}\left(W_{N_2,in} - W_{N_2,out}\right), \end{aligned} \tag{8}$$

where R_{O_2} and R_{N_2} represent oxygen gas constant and nitrogen gas constant respectively, M_{O_2} and M_{N_2} represent the molar mass of oxygen and nitrogen, T_{st} and V_{ca} are the temperature and volume of PEMFC respectively, $W_{O_2,in}$ and $W_{N_2,in}$ are given by

$$\begin{aligned} W_{O_2,in} &= W_{s,out}\frac{1}{1+\omega_{vap}}x_{O_2,in}, \\ W_{N_2,in} &= W_{s,out}\frac{1}{1+\omega_{vap}}(1 - x_{O_2,in}), \end{aligned} \tag{9}$$

where ω_{vap} is the oxygen mass fraction of water in the air, $x_{O_2,in}$ is the mass fraction in dry gas. Then

$$W_{O_2,con} = M_{O_2} \times \frac{nI_{st}}{2F}, \tag{10}$$

where n is number of cells, F is Faraday number, I_{st} is PEMFC load current, and

$$\begin{aligned} W_{O_2,out} &= W_{ca,out}x_{O_2,out}, \\ W_{N_2,out} &= W_{ca,out}(1 - x_{O_2,out}), \end{aligned} \tag{11}$$

where $x_{O_2,out}$ is the oxygen mass fraction of exhaust gas,

$$x_{O_2,out} = \frac{M_{O_2}P_{O_2}}{\kappa p_{ca}}, \tag{12}$$

where κ is a constant [5], $W_{ca,out}$ is the rate of gas flow out the stack and can be described in high pressure PEMFC system by

$$W_{ca,out} = \theta\frac{C_d A_1 p_{ca}}{\sqrt{RT_{st}}}\sqrt{\gamma\left(\frac{2}{\gamma+1}\right)^{\frac{\gamma}{\gamma-1}}}, \tag{13}$$

where C_d is discharge coefficient, A_1 and θ are opeing area and opening degree of proportional back pressure valve respectively, R is universal gas constant.

3 Objective Optimization

The focus of the air supply system is to avoid oxygen starvation and provide maximum net power. Generally, with increasing flow rates into the cathode and cathode pressure, the total power, p_{st}, generated by stack will increase when the parasitic power of accessories is not considered and can be defined by

$$p_{st} = V_{st}I_{st} \tag{14}$$

where V_{st} is the fuel cell voltage. Since the stack is made up of a plurality of individual fuel cells connected in series, the voltage of the fuel cell is equaled to the number, n, of individual fuel cells multiplied by single cell voltage, V_{fc}.

$$V_{st} = n \times V_{fc} \tag{15}$$

where V_{fc} can be written as

$$V_{fc} = E_{ns} - V_{act} - V_{ohm} - V_{conc} \tag{16}$$

where nernst voltage, E_{ns}, is a positive correlation function of cathode pressure, p_{ca}, oxygen partial pressure, p_{O_2}, and hydrogen partial, p_{H_2}. V_{act}, V_{ohm}, V_{conc} represent the voltage of activation loss, ohmic loss, concentration loss respectively. According to the Eqs. (14), (15), (16), the power of the fuel cell increases with the increase of flow rate and cathode pressure. However, increasing the flow rate and cathode pressure not only increases the power of the fuel cell, but also increases the parasitic power generated by the compressor and other accessories. Because the parasitic power generated by the compressor accounts for a large proportion of the total parasitic power, this paper assumes that the compressor is the only accessory that produces parasitic power, p_{pr}, which can be calculated by

$$p_{pr} = V_{cm} \times \frac{V_{cm} - g_a\omega_{cm}}{R_{cm}}, \tag{17}$$

so the net power of PEMFC is described as

$$p_{net} = p_{st} - p_{pr}, \tag{18}$$

so the net power is determined by the total power of the fuel cell and the parasitic power.

As shown in the Figure 3, the net power shows a non-monotonous trend with the increase of flow rate and cathode pressure when load current is set at 120A. To obtain the optimal reference flow rate and cathode pressure, under different operating conditions, open-loop model simulation experiments have been carried out. The net power of the PEMFC stack is obtained by measuring the load current, I_{st}, stack voltage, V_{st}, compressor voltage, V_{cm}, and angular velocity, ω_{cm}, of compressor. The maximum net power indexed by flow rate and cathode pressure. Then inputting the load current, the optimal flow rate and cathode pressure can be expressed based on map.

4 CONTROL DEVELOPMENT

The main control objective is to achieve maximum net power and avoid oxygen starvation. For fuel cell air supply subsystem, multivariable control involves fixed point control of flow rate, $W_{s,out} = W_e$, and fixed point control of cathode pressure, $p_{ca} = p_e$. According to Eq. (5), $W_{s,out}$ is the positive proportional function of the difference between p_{sm} and p_{ca}, and the nozzle constant k_{sc} is a constant. Therefore, the control targets are selected as $y_{d1} = p_e$ and $y_{d2} = \frac{W_e}{k_{sc}}$. According to the work done in the section III, mark tracking targets y_{d1} and y_{d2} as

$$y_{d1} = f_1(I_{st}), \tag{19}$$

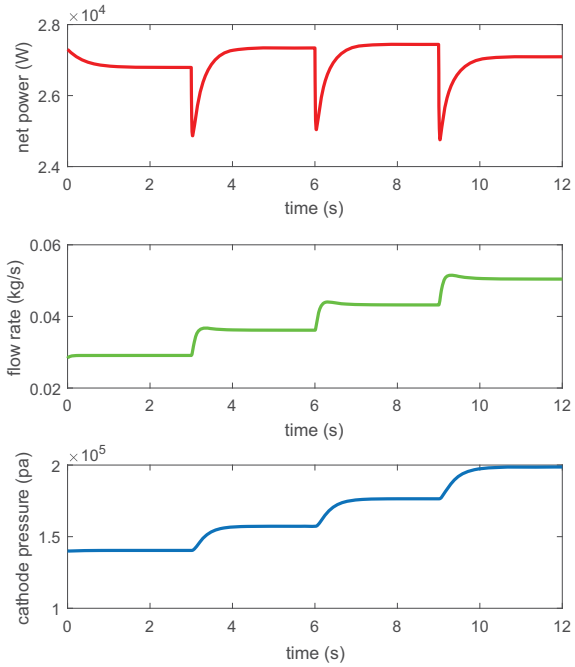

Figure 3: Maximum net power distribution

$$y_{d2} = f_2(I_{st}). \tag{20}$$

In order to get good tracking performance, coordinately controlling the voltage of the compressor and the opening degree of proportional back pressure valve is necessary. In the actual system, the voltage of the compressor is ranging from 50V to 250V, and the dimensionless proportional back pressure valve opening degree is ranging from 0 to 1. Due to the serious nonlinear characteristics of air supply subsystem described in section II, this paper proposes a strategy combining target optimization and a nonlinear control method called triple-step control as shown in Figure 4. The triple-step method, combining steady-state, feedforward and error feedback control, has a good control effect on nonlinear systems.

According to the air supply system model established in the section II, a third-order nonlinear state space equation is obtained by

$$\begin{aligned}
\dot{x}_1 &= -a_1 x_1 - \frac{a_2}{x_1}\left[\left(\frac{x_2}{a_3}\right)^{a_4} - 1\right] \\
&\quad \times f(x_1, x_2) + a_5 u_2, \\
\dot{x}_2 &= a_6\left[1 + a_7\left[\left(\frac{x_2}{a_3}\right)^{a_4} - 1\right]\right] \\
&\quad \times \left[f\left(x_1, x_2\right) - a_8\left(x_2 - x_3\right)\right], \\
\dot{x}_3 &= \left(a_9 + a_{10}\right)\left(x_2 - x_3\right) \\
&\quad + \left(\frac{a_{11}a_{12}a_{13}}{\kappa} - \frac{a_{12}a_{13}}{\kappa}x_3\right) u_1 - a_{14} I_{st},
\end{aligned} \tag{21}$$

where $[u_1, u_2,]^T \triangleq [\theta, V_{cm}]^T$, $a_i (i = 1, 2 \cdots 14)$ are known constants calculated by the physical quantities in section II, $x = [x_1, x_2, x_3]^T \triangleq [\omega_{cm}, p_{sm}, p_{ca}]^T$.

Defining the output $y_1(t)$ and $y_2(t)$ of the system as

$$y_1(t) = p_{ca}, \tag{22}$$

$$y_2(t) = p_{sm} - p_{ca}, \tag{23}$$

where p_{sm} and p_{ca} are both measurable state variables. By taking the time derivative of $y_1(t)$, we obtain

$$\begin{aligned}
\dot{y}_1(t) &= \left(a_9 + a_{10}\right)\left(x_2 - x_3\right) \\
&\quad + \left(\frac{a_{11}a_{12}a_{13}}{\kappa} - \frac{a_{12}a_{13}}{\kappa}x_3\right) u_1 - a_{14} I_{st},
\end{aligned} \tag{24}$$

To simplify the formula, introduce $\phi_1(t)$ and $\psi_{11}(t)$

$$\begin{aligned}
\phi_1(x) &= \left(a_9 + a_{10}\right)\left(x_2 - x_3\right) - a_{14} I_{st} \\
\psi_{11}(x) &= \frac{a_{11}a_{12}a_{13}}{\kappa} - \frac{a_{12}a_{13}}{\kappa}x_3
\end{aligned} \tag{25}$$

and then taking the time derivative of $y_2(t)$

$$\begin{aligned}
\dot{y}_2(t) &= \dot{x}_2 - \dot{x}_3 \\
&= a_6[1 + a_7[(\frac{x_2}{a_3})^{a_4} - 1]] \\
&\quad \times [f(x_1, x_2) - a_8(x_2 - x_3)] - \dot{x}_3.
\end{aligned} \tag{26}$$

again, introduce $h(x_2)$

$$h(x_2) = a_6[1 + a_7[(\frac{x_2}{a_3})^{a_4} - 1] \tag{27}$$

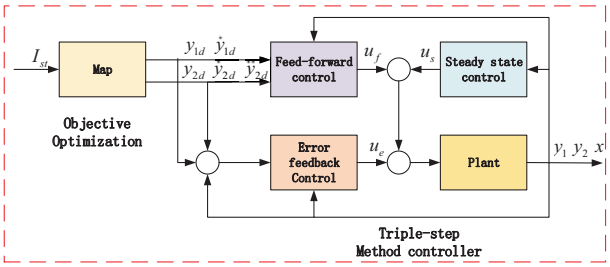

Figure 4: Structure of tracking target optimization combined with a triple-step method controller.

4.1 Reference Generator

According to the Eqs. (19), (20), (22), (23), defining tracking error $e_1 \triangleq y_1(t) - y_{1d}$ and $e_2 \triangleq y_2 - y_{2d}$. By taking the time derivative of e_2, we can obtain

$$\dot{e}_2 = h(x_2)[f(x_1, x_2) - a_8(x_2 - x_3)] - \dot{x}_3 - \dot{y}_{2d}, \tag{28}$$

and then defining virtual variable υ_s,

$$\upsilon_s = h(x_2)[f(x_1, x_2) - a_8(x_2 - x_3)] - \dot{y}_{2d}, \tag{29}$$

so

$$\dot{e}_2 = \upsilon_s - \dot{x}_3. \tag{30}$$

Defining the virtual reference variable:

$$\upsilon_{sr} = -k_2 e_2 + \dot{x}_3, \tag{31}$$

and virtual variable error

$$e_3 = \upsilon_s - \upsilon_{sr}, \tag{32}$$

By taking the time derivative of υ_s, we can obtain

$$\begin{aligned}
\dot{\upsilon}_s &= \frac{\partial h(x_2)}{\partial x_2}\dot{x}_2[f(x_1, x_2) - a_8(x_2 - x_3)] \\
&\quad + h(x_2)[\frac{\partial f(x_1, x_2)}{\partial x_1}\dot{x}_1 + \frac{\partial f(x_1, x_2)}{\partial x_2}\dot{x}_2 \\
&\quad - a_8(\dot{x}_2 - \dot{x}_3)] - \ddot{y}_{2d} \\
&= \phi_2(x) + \psi_{21}(x)u_1 + \psi_{22}(x)u_2,
\end{aligned} \tag{33}$$

where

$$\phi_2(x) = (\frac{\partial h(x_2)}{\partial x_2}[f(x_1,x_2) - a_8(x_2 - x_3)] + h(x_2)[\frac{\partial f(x_1,x_2)}{\partial x_2} - a_8])\dot{x}_2 + h(x_2)\frac{\partial h(x_1,x_2)}{x_1} (-a_1 x_1 - \frac{a_2}{x_1}[(\frac{x_2}{x_{11}}^{a_4}) - 1]f(x_1,x_2)), \tag{34}$$

and

$$\psi_{21}(x) = a_8 h(x_2)\psi_{11}(x) \quad \psi_{22}(x) = a_5 h(x_2)\frac{\partial f(x_1,x_2)}{x_1} \tag{35}$$

4.2 Triple-Step Design

The general expression of the triple-step control law of the multi-input and multi-output system is as follows

$$u = u_s + u_f + u_e, \tag{36}$$

where steady state control u_s:

$$u_s = \begin{bmatrix} u_{s1} \\ u_{s2} \end{bmatrix} = -\begin{bmatrix} \psi_{11}(x) & 0 \\ \psi_{21}(x) & \psi_{22}(x) \end{bmatrix}^{-1} \begin{bmatrix} \phi_1(x) \\ \phi_2(x) \end{bmatrix}, \tag{37}$$

and reference feedforward control u_f:

$$u_f = \begin{bmatrix} u_{f1} \\ u_{f2} \end{bmatrix} = -\begin{bmatrix} \psi_{11}(x) & 0 \\ \psi_{21}(x) & \psi_{22}(x) \end{bmatrix}^{-1} \begin{bmatrix} \dot{y}_{1d} \\ \dot{y}_{2d} \end{bmatrix}, \tag{38}$$

then error feedback control u_e:

$$u_e = \begin{bmatrix} u_{e1} \\ u_{e2} \end{bmatrix} = -\begin{bmatrix} \psi_{11}(x) & 0 \\ \psi_{21}(x) & \psi_{22}(x) \end{bmatrix}^{-1} \begin{bmatrix} k_1 e_1 \\ e_2 + k_3 e_3 \end{bmatrix}. \tag{39}$$

4.3 Proof of Stability

Defining the Lyapunov function

$$V = \frac{1}{2}[e_1^2 + e_2^2 + e_3^2]. \tag{40}$$

Based on Eqs. (24)∼(40), take the time derivative of V, we obtain

$$\begin{aligned} \dot{V} &= e_1[\phi_1(x) + \psi_{11}(x)u_1 - \dot{y}_{1d}] \\ &\quad + e_2(\upsilon_s - \upsilon_{sr}) + e_2\upsilon_{sr} - e_2\dot{x}_3 + e_3(\upsilon_s - \dot{\upsilon}_{sr}) \\ &= e_1[\phi_1(x) + \psi_{11}(x)u_1 - \dot{y}_{1d}] + e_2 e_3 - k_2 e_2^2 \\ &\quad + e_3[\phi_2(x) + \psi_{21}(x)u_1 + \psi_{22}(x)u_2 - \dot{\upsilon}_{sr}], \end{aligned} \tag{41}$$

further finishing Eq. (40) can get the following formula

$$\begin{aligned} \dot{V} &= -k_2 e_2^2 + [e_1 \quad e_3]\begin{bmatrix} \phi_1(x) - \dot{y}_1 \\ \phi_2(x) + e_2 - \dot{\upsilon}_{sr} \end{bmatrix} \\ &\quad + [e_1 \quad e_3]\begin{bmatrix} \psi_{11}(x) & 0 \\ \psi_{21}(x) & \psi_{22}(x) \end{bmatrix}\begin{bmatrix} u_1 \\ u_2 \end{bmatrix} \\ &= -k_1 e_1^2 - k_2 e_2^2 - k_3 e_3^2 < 0. \end{aligned} \tag{42}$$

Based on Eqs. (42), we prove the stability of the controller.

Table 1: Parameters

J_{cm}	0.0005 $kg \cdot m^2$
η_{cm}	0.98
g_a	0.153 $V/(rad/sec)$
g_b	0.153 $N - m/Amp$
R_{cm}	0.9 Ω
C_p	1004 $J/(mol \cdot K)$
T_{atm}	298.15 K
p_{atm}	101325 pa
η_{cp}	0.8
γ	1.4
R_a	286.9 $J/(kg \cdot K)$
V_{sm}	$0.02m^3$
k_{sc}	$0.3629 \times 10^{-5} kg/(s \cdot pa)$
R_{O_2}	259.8 $J/(kg \cdot K)$
T_{st}	380 K
V_{ca}	$0.01m^3$
M_{O_2}	0.032 kg/mol
R_{N_2}	296.8 $J/(kg \cdot K)$
M_{N_2}	0.028 kg/mol
ω_{vap}	0.2
$x_{O_2,in}$	0.232
n	400
I_{st}	A
F	96485 coulombs
C_d	0.0124
A_1	0.002 m^2
R	8.3145 $J/(mol \cdot K)$

5 Results and Analysis

The control law proposed in the previous section was tested in the simulation model given in Section II. The parameters used in the simulation are as shown in Table. 1. In order to verify the effectiveness of the designed controller, this paper establishes a simulation model and designs the controller in Matlab/Simulink environment.

Since the power demand is generally step-change in actual fuel cell engine systems, the solid red line indicates the required step-change load current as shown in Figure 5, where the load current is considered as a measurable disturbance. In Figure 6 and Figure 7, red solid lines correspond to the optimal cathode pressure and pressure difference between air supply manifold and cathode under the different load current, respectively. As Figure 6, The blue dotted line shows the cathode pressure obtained from simulation model that incorporates the controller. At the third and eighth seconds, the load current and the given optimal cathode pressure change stepwise at the same time and the system can respond quickly and track target due to the combination of feedforward control law and error feedback control law. And under the action of the steady-state control law and the error feedback control law, there is no steady-state tracking error. In Figure 7, the green dotted line indicates the difference between the air supply manifold pressure and the cathode pressure of the simulation model. In the process of dynamic tracking, the actual output of the system first presents an opposite trend to the optimal value, then quickly responds and tracks the given optimal value. This condition is caused by the rapid increase of cathode pressure resulting in the de-

crease of pressure difference and the result is reasonable because the response of the proportional back pressure valve is much faster than the compressor.

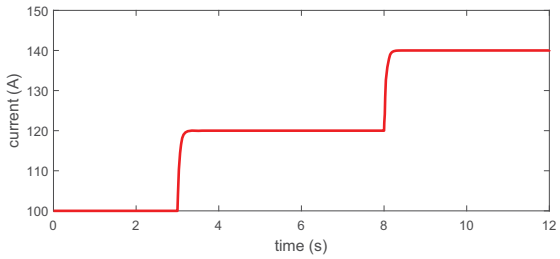

Figure 5: Given load current

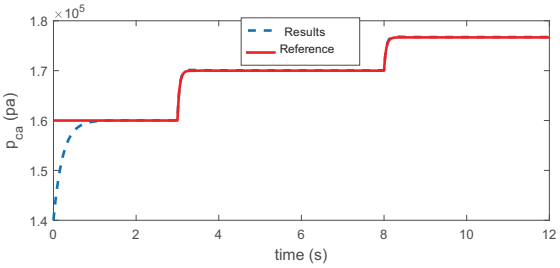

Figure 6: Control effect of the cathode pressure, p_{ca}, under the optimal values

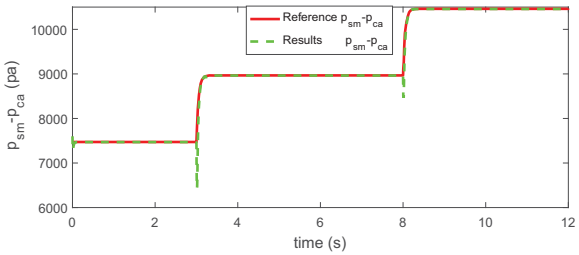

Figure 7: Control effect of the difference between air supply manifold pressure and cathode pressure, $p_{sm} - p_{ca}$, under the optimal values

6 Conclusion

This paper establishes a MIMO fuel cell air supply subsystem model which is simplified based on the electrochemistry and gas dynamics. Based on fuel cell net power, optimize tracking targets and then gain the optimal target under different load currents through a map. Finally, a nonlinear control strategy called triple-step method is proposed. The stability of the closed-loop system is proved by the Lyapunov-based method. The simulation results show that the designed controller presents good performance in terms of tracking the target cathode pressure and air flow.

References

[1] G. Jinwu, L. Meng, H. Yunfeng, C. Hong, M. Yan, Challenges and developments of automotive fuel cell hybrid power system and control, SCIENCE CHINA Information Sciences, doi:10.1007/s11432-018-9690-y.

[2] R. Tirnovan, S. Giurgea, Efficiency improvement of a pemfc power source by optimization of the air management, International Journal of Hydrogen Energy, 37(9): 7745–7756, 2012.

[3] J. T. Pukrushpan, Modeling and control of fuel cell systems and fuel processors, Dissertation Abstracts International, Volume: 64-02, Section: B, page: 0925.;Chairs: Anna Stefanopo, 18(3): 594–6, 2003.

[4] M. Grujicic, K. M. Chittajallu, E. H. Law, J. T. Pukrushpan, Model-based control strategies in the dynamic interaction of air supply and fuel cell, Proceedings of the Institution of Mechanical Engineers.part A.journal of Power & Energy, 218(7): 487–499, 2004.

[5] R. J. Talj, D. Hissel, R. Ortega, M. Becherif, M. Hilairet, Experimental validation of a pem fuel-cell reduced-order model and a moto-compressor higher order sliding-mode control, IEEE Transactions on Industrial Electronics, 57(6): 1906–1913, 2010.

[6] C. Jian, Z. Liu, W. Fan, O. Quan, H. Su, Optimal oxygen excess ratio control for pem fuel cells, IEEE Transactions on Control Systems Technology, PP(99): 1–11, 2017.

[7] C. Kunusch, P. F. Puleston, M. A. Mayosky, J. Riera, Sliding mode strategy for pem fuel cells stacks breathing control using a super-twisting algorithm, IEEE Transactions on Control Systems Technology, 17(1): 167–174, 2008.

[8] J. K. Gruber, C. Bordons, A. Oliva, Nonlinear mpc for the airflow in a pem fuel cell using a volterra series model, Control Engineering Practice, 20(2): 205–217, 2012.

[9] A. Aldurra, S. Yurkovich, Y. Guezennec, Study of nonlinear control schemes for an automotive traction pem fuel cell system, International Journal of Hydrogen Energy, 35(20): 11291–11307, 2010.

[10] Y. B. Kim, Improving dynamic performance of proton-exchange membrane fuel cell system using time delay control, Journal of Power Sources, 195(19): 6329–6341, 2010.

[11] R. D. Fonseca, E. Bideaux, M. Gerard, B. Jeanneret, M. Desbois-Renaudin, A. Sari, Control of pemfc system air group using differential flatness approach: Validation by a dynamic fuel cell system model, Applied Energy, 113(6): 219–229, 2014.

[12] Q. Li, W. Chen, Y. Wang, J. Jia, M. Han, Nonlinear robust control of proton exchange membrane fuel cell by state feedback exact linearization, Journal of Power Sources, 194(1): 338–348, 2009.

[13] DANZER, A. Michael, WILHELM, Jorg, ASCHEMANN, Harald, HOFER, P. Eberhard, Model-based control of cathode pressure and oxygen excess ratio of a pem fuel cell system, Journal of Power Sources, 176(2): 515–522, 2008.